Steel-Sense: Integrating Machine Elements with Sensors by Additive Manufacturing

Tatyana Vasilevitsky
The Hebrew University of Jerusalem
Jerusalem, Israel
tatyana.vasilevitsk@mail.huji.ac.il

Amit Zoran
The Hebrew University of Jerusalem
Jerusalem, Israel
zoran@cs.huji.ac.il

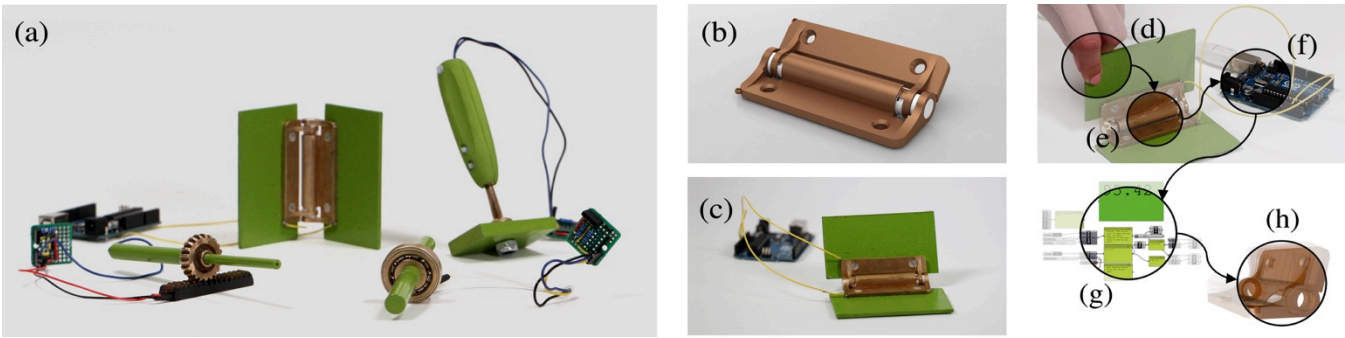

Figure 1. (a) Steel-Sense: four 3D-printed metal machine elements augmented with sensing abilities. From left to right: a voltage divider integrated inside a gear; a variable capacitor embedded in a hinge; an electronic switch within a ball bearing; and a pressure sensor within a screw (and its dedicated screwdriver). For example: (b) the virtual model of the hinge (rendered with VRay), and (c) the 3D-printed hinge system. An operation scenario: (d) a change in the hinge's opening angle (e) changes its capacitance. (f) An Arduino microcontroller measures the resulting capacitance. (g) A Grasshopper script uses the output data (h) to control the virtual model, mirroring the physical hinge.

ABSTRACT
Many interactive devices use both machine elements and sensors, simultaneously but redundantly enabling and measuring the same physical function. We present Steel-Sense, an approach to joining these two families of elements to create a new type of HCI design primitive. We leverage recent developments in 3D printing to embed sensing in metal structures that are otherwise difficult to equip with sensors, and present four design principles, implementing (1) an electronic switch integrated within a ball bearing; (2) a voltage divider within a gear; (3) a variable capacitor embedded in a hinge; and (4) a pressure sensor within a screw. Each design demonstrates a different sensing principle, and signals its performance through (1) movement; (2) position; (3) angle (4) or stress. We mirror our elements physical performance in a virtual environment, evaluate our designs electronically and structurally, and discuss future work and implications for HCI research.

CHI'16, May 07-12, 2016, San Jose, CA, USA

DOI: http://dx.doi.org/10.1145/2858036.2858309

Author Keywords
3D Printing; Sensors; Digital Fabrication; Hybrid Design; Machine Elements; Additive Manufacturing; Metal Printing.

ACM Classification Keywords
H.5.2 Information interfaces and presentation: User Interfaces - Input devices and strategies.

INTRODUCTION
Sensors and machine elements are key components in the construction of many interactive devices. Machine elements determine the potential of a device's physical freedom, while sensors measure the actual use of this potential. Although sensor design is a common research field within HCI (see the Related Work section), the study of machine elements seems foreign to traditional HCI, where many researchers use off-the-shelf components in developing their projects. Furthermore, in many designs these two families of elements are used together, but the integration between them has not been explored, as designers still rely on traditional separation between machine elements and sensors. We wish to study the possibility of merging these two families of components, seeking to use both efficiently (saving space and material), and forming a new interactive space in HCI.

Like sensors, machine elements come in a variety of types and meet a wide range of needs, satisfying structural requirements, and controlling motion and/or user mechanical input [21]. Bearings, axles, seals, gears, screws

and other elements are produced in mass quantities, reducing their cost to bare minimum. While offering an extensive portfolio of designs, the industrial standards that dictate the forms and dimensions of such elements limit design freedom, introducing rigid constraints on the making process. In the realm of customization enabled by digital fabrication, the *need* to constrain the design process with rigid standards and catalogues seems out-of-date.

Additive Manufacturing (AM) calls for a revision of traditional disciplinary boundaries [3], enabling designers to produce specific solutions for specific needs. AM of metal parts makes conductive objects that can be used to 3D print sensors, and complicated 3D structures that can be used to 3D print machine elements [15]. This creates an opportunity to bridge mechanical design with sensors, and link the research in 3D-printed mechanisms with that of digitally fabricated sensors. Thus, with Steel-Sense we are motivated to free the design of sensor and machine elements from industrial standards, integrating sensors into structures with complex physical constraints using existing AM material and processes. Additionally, Steel-Sense contributes a new family of *double agent* elements—*facilitating mechanical performance while evaluating the same performance*.

With Steel-Sense, mechanical actions (such as angular and linear movement, motion transmitting, and structural alignments) and sensorial (electromagnetic) measurements are considered as a single performing unit, rather than simply combining sensors with machine elements as current solutions offer [7,18]. We envision these hybrid elements impacting the traditional design of interactive systems, as they offer a new interactive vocabulary of *performing* and *measuring* in a single unit.

In this paper, we span our new design space using four fundamental Steel-Sense principals, illustrated by the combination of fundamentally different machine elements and sensing capabilities. As the components described below are likely the most common machine elements, they are the best suited to establishing the Steel-Sense concept, rather than suggesting specific products. In the present work, we emphasize the technology (see Fig. 1) of a Steel-Sense (1) ball bearing; (2) gear; (3) hinge; and (4) screw. We 3D printed (1) a differential *rotary motion* detector for a ball bearing using an embedded switch; (2) a differential *linear motion* detector with a voltage divider embedded in a linear gear; (3) an *angle detector* using a variable capacitor in the shape of a hinge axle, and (4) an embedded sensing mechanism to measure *force* applied to a screw. We evaluated the structural performance of the new designs with the Finite Element Method (FEM), and also ran electronic performance measurements and analysis. A future work will broaden the discussion on HCI implications; here, we discuss the potential of several HCI applications based on our current design-cases.

This paper is structured around a presentation of the new designs, followed by structural and signal evaluation for each of the four machine elements. In the next section, we review related work, before presenting the technology itself in the Steel-Sense section. We discuss implications to HCI before concluding the work in the last section.

RELATED WORK

Several recent 3D printing projects have demonstrated designs with a high degree of mechanical freedom [28,29]. Along the same lines, Schmitt offers a parametric design procedure to customize 3D-printed machine parts, taking into consideration the specifications (tolerance, resolution) of a given 3D printing technology [10]. Yet in many cases, designers and engineers are bound to traditional design paradigms, paralleling mechanical and sensorial systems instead of merging them. For example, in [12] the researchers 3D printed two parallel gear systems. One converted a servomotor's rotary motion to linear motion, while a second measured movement on the same axis. While these parallel systems are common within traditional practices, 3D printing metal structures allows us to hybridize such systems, developing specific solutions while reducing cost and space.

In HCI, researchers have already started to explore the intersection of 3D printing and interactive components, as in the 3D-printed optics by Willis et al. [27]. In the last several years a vast body of work has been published on 2D-printed (customizable) electronics and sensors [4,7,9,14], and we can expect the development of fully functional 3D-printed electronics, likely beginning with conductive traces layered on a 3D model, etc., as suggested by Voxel8 [16]. In our work, we propose several interactive design primitives. This approach, of suggesting a new interaction potential using a finite set of interactive grammars, is common within HCI research, as seen in projects such as Sticky Actuator [21] and PneUI [26].

STEEL-SENSE

Steel-Sense presents four different 3D-printed machine elements integrated with four different sensing capabilities. These elements produce electronic signals echoing their mechanical performance. A ball bearing, a gear, a hinge, and a screw (plus a screwdriver) were designed to perform as similarly as possible to traditional machine elements, yet with small structural changes that enable them to function as motion, angle, and pressure sensors.

Design and Fabrication

Currently there are several AM technologies available from online services that enable digital fabrication of metal parts. The high-end process offered by *Stratasys* provides full sintering of metal powder using Direct Metal Laser

Sintering (DMLS) for stainless steel, titanium, aluminum and other alloys [13]. While this is a costly process (see below), cheaper options are available from *Shapeways* [11] and *i.materialize*. A hybrid printing/casting option is offered for metals with lower melting points, such as brass, bronze, silver, and gold. These materials can be easily cast from 3D-printed wax models. An even cheaper hybrid option (with probably the lowest resolution) digitally layers steel powder (60%) and deposits it with melted bronze (40%).

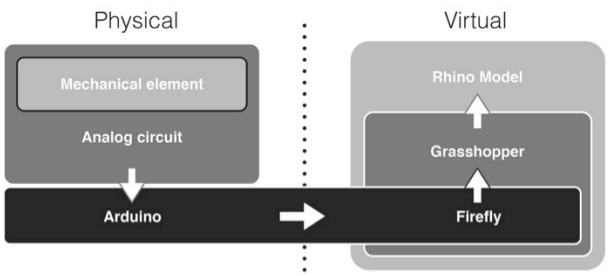

Figure 2. The data from the physical element and its circuit affect the virtual model in Rhino, flowing through Arduino and Firefly to Grasshopper.

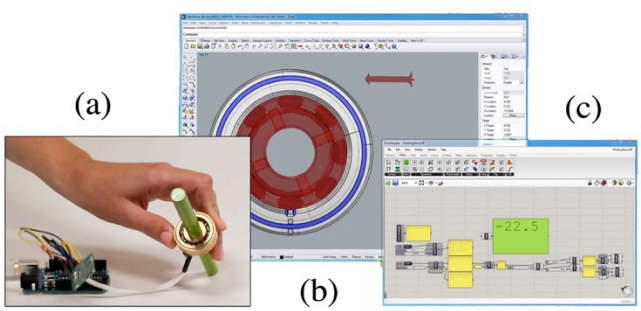

Figure 3. Dataflow from the physical machine element (ball bearing) (a) to the virtual model (b) using Grasshopper (c), Firefly and Arduino.

We compare the costs, as of August 25, 2015, of the same part (one of the hinge pieces) with the three technologies. Stratasysdirect DMLS Stainless Steel varies from $419 (Stainless Steel 17-4PH) to $457 (Stainless Steel 316L) for a single print. Raw bronze costs $63.63 (Shapeways) or $75.55 (i.materialise), while a steel/brass hybrid costs $22.76 (Shapeways) or $25.85 (i.materialise). The detailed specifications and accuracy of these processes can be found in the references. Generally speaking, the DMLS process is lower in resolution than wax printing, but post-print surface treatment can achieve a very smooth result.

All of our metal parts were designed in Rhino and 3D printed in wax, then made in bronze. While DMLS Stainless Steel is a superior AM process for our application, due to its significantly higher production cost we demonstrate our designs using a less expensive, less durable metal. Plastic parts (insulators) were printed by Shapeways using Selective Laser Sintering (SLS) of nylon 12 (the cost of SLS nylon is negligible compared to metal prints). To integrate capacitance and resistance into our designs, we use special SLS materials offered by Stratasysdirect: NyTek™ 1200 GF (nylon 12 plus glass for a higher dielectric constant) and NyTek™ 1200 CF (nylon 12 plus carbon for a weak conductivity). A detailed design for each element is presented below in the corresponding sections.

In addition to the mechanical designs, we implement analog circuits to read data from the sensors using an Arduino board. The data is transferred from the Arduino to a PC via USB (using the Arduino's serial port). Virtual models (in Rhino) mirror the physical performance of the machine element through Grasshopper (a parametric plug-in to Rhino) and Firefly (a Grasshopper plugin for Arduino integration, see Fig. 2 and Fig. 3).

Principals of Elements Evaluation

As we revise well-known elements with stable performance, it is necessary to visualize how our design affects them structurally. To evaluate the mechanical performance of our design (as presented in each section), we ran FEM simulations for each part using Scan&Solve (an FEM plugin for Rhino). We discuss the structural implication of our new designs below. For the simulations, we assumed these elements were printed in DMLS Stainless Steel 17-7 (which is superior to bronze for most real applications), and compare our hybrid designs to traditional ones made from the same material. We intentionally pushed the simulation to extreme (failure) conditions, comparing our designs to traditional components under the same conditions to easily visualize differences in failure performance. More advanced structural evaluation is needed in the future, as we present only our initial results here.

Machine Element (1): A Switch Ball Bearing

Our first hybrid element is a ball bearing (Fig. 3-4): a bearing mechanism between a fixed axle and a rotating part, separated by a ring of small balls that reduce rotational friction and support loads. Ball bearings come in a diverse range of shapes and sizes, and can be made from a variety of metals, plastics, and even ceramics. Bearings are fundamental in any mechanical design with degrees of freedom, as they allow movement. While we relied on a common ball bearing design, our solution will also fit alternative ball bearings.

Our ball bearing (printed from bronze and nylon 12, 17.1 mm radius, 10.3 mm wide) implements a differential angular motion detector in the form of a two-way single pole switch (Fig. 4e), counting quarter circles (90 degrees rotations). The outer ring supports the whole inner structure, and encloses two isolated side rings (see Fig. 4a-b). Each of these side rings has four pins (90 degree from each other, Fig. 4c) inside, but isolated from, the outer ring. A nylon case sets the angle between the inner ring and the balls.

The outer ring of the ball bearing is grounded at all times. Both side rings are supplied with a voltage of 5V, and each is

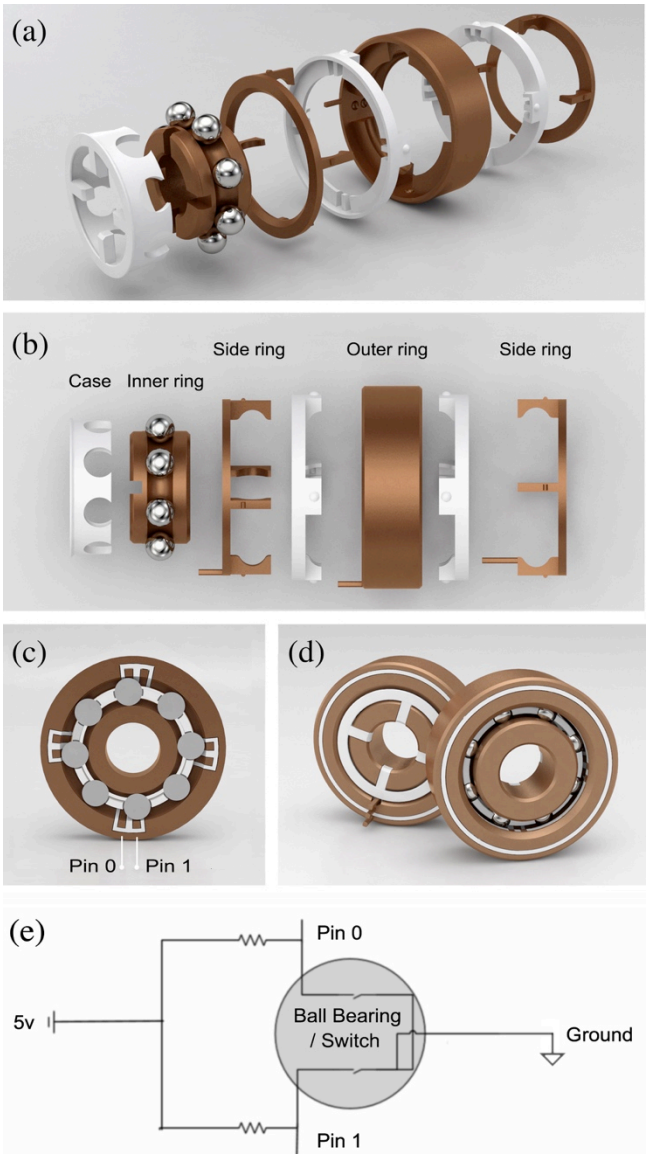

Figure 4. (a-d) The design of the 3D printed switch ball bearing using bronze, nylon, and steel balls. (e) The analog circuit design. Rendered in VRay.

connected to an analog pin on the microcontroller. During the rotation of the ball bearing, contact with the outer ring may be made by either pin (or both simultaneously). When the outer ring makes contact, the current flows to ground through a resistor, bringing the analog pin from 5V to ground. To best evaluate the performance of our ball bearing, we use analog data polling to monitor the voltage on the pins. However, digital polling may be preferred for some practical applications.

In the firmware, the angle counter is set to 0 on the ball upon initiation. The firmware samples the analog pins periodically and detects the contact between the side and the outer ring. We use a sequence of input samples to determine the rotation angle and angular speed. We use

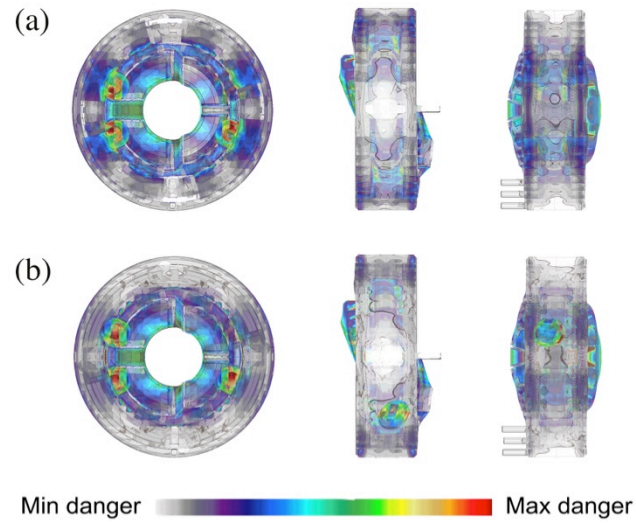

Figure 5. FEM simulation of torque (500KNm) applied to the inner ring, aligned with the ball bearing rotation plane, tested on our ball bearing switch design (a) and compared to a standard design (b). Colors represent risk (danger) to structural integrity.

$(P_i^{\{H,L\}},T)$ to describe the state of pin $i \in [0,1]$ at time T, when $\{H,L\}$ represent High/Low. For example, (P_0^H,T) means Pin 0 is High at time T, and the notation $<(P_0^{\{H,L\}},T),(P_1^{\{H,L\}},T)>$ describes the state of both pins at a given time T, thus describing the whole system. Using this notation, we can describe clockwise rotation with the following series (by switching the states of the two pins, we describe counterclockwise rotation):

contact with pin 0	**contact with both pins**	**contact with pin 1**
$<(P_0^L,t),(P_1^H,t)>$	$<(P_0^L,t+1),(P_1^L,t+1)>$	$<(P_0^H,t+2),(P_1^L,t+2)>$

The firmware running on the Arduino polls the state of the pins and attempts to find a series as described above. Arduino's analog resolution is 1024, with the values [0:1024] representing voltage values of 0-5V. For our purposes, anything in the lower half of the resolution ([0:512] will be taken as low, and the rest of the values will be high. The program samples the inputs once every 5ms and averages the reading from the last 10 samples, in order to reduce noise. Each instance of the described series indicates 1/4 turn. We set the orientation such that clockwise rotation is counted as (+1), and counterclockwise as (-1). The resulting sum is the number of 1/4 turns made by the ball bearing, which is the data output to the serial port. Grasshopper uses this output to rotate the ball bearing model and display the angle of rotation.

Ball Bearing Performance

FEM simulation is used to evaluate the new design. We simulate a torque on the inner ring, aligned with the ball

bearing rotation plane. In Fig. 5 we present the results of two designs: the first is our ball bearing switch, and the second is a similar, more traditional, design with a unified outer ring, rather than separate side and outer rings.

The two simulations have similar results: i.e., the new design does not introduce a significant risk caused by static torque. Nevertheless, manual operation of the ball suggests a friction problem, as the rotation of the inner part is not smooth. This is a direct result of the lower accuracy of the 3D printed process compared to the professional standards of ball bearings, and can be improved by accurate post-machining.

For the electrical output, we note a tradeoff of reliability versus stability. As the angular speed increases, a higher sampling frequency is required to catch the voltage transitions. However, the greater sampling rate introduces an increasing amount of noise, which can be reduced with better surface contact, as noted in *Design Process and Constraints*. Fig. 6 shows the voltage output for both pins for different speeds of rotation over a few seconds and a complete turn, with a sampling rate of 13.333 Hz.

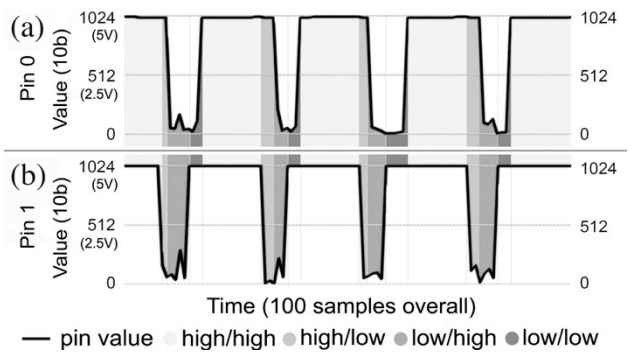

Figure 6. Voltage outputs measured by two Arduino pins (a-b), over 100 samples taken with a 75ms sampling interval. The gray key represents logic state.

Machine Element (2): A Voltage Divider Gear

A gear is a set of toothed elements, either wheels or linear bars that work together to transfer one type of driving force to another. While the applications for gears are innumerable, here we present a simple system with a wheel and a linear gear that transfers rotation to linear motion. We revise a traditional linear gear (the *track*, 67 x 8.5 x 11.9 mm) by separating it into four alternating-tooth systems, connected together to a single housing using NyTek™ 1200 CF (nylon 12 with carbon) SLS. The main industrial use of NyTek™ 1200 CF is to improve the thermal performance of nylon 12 as a common SLS material. However, the conductivity of the carbon also makes it a good resistor [1], allowing us to implement a voltage divider between the four alternating-tooth systems.

In essence, the gear moving on the track functions as a potentiometer—by changing the resistance of the circuit as it moves on the track, it also changes the voltage on the wheel. The track consists of repeated sequences of three resistors connected in series. This design creates voltage dividers on the

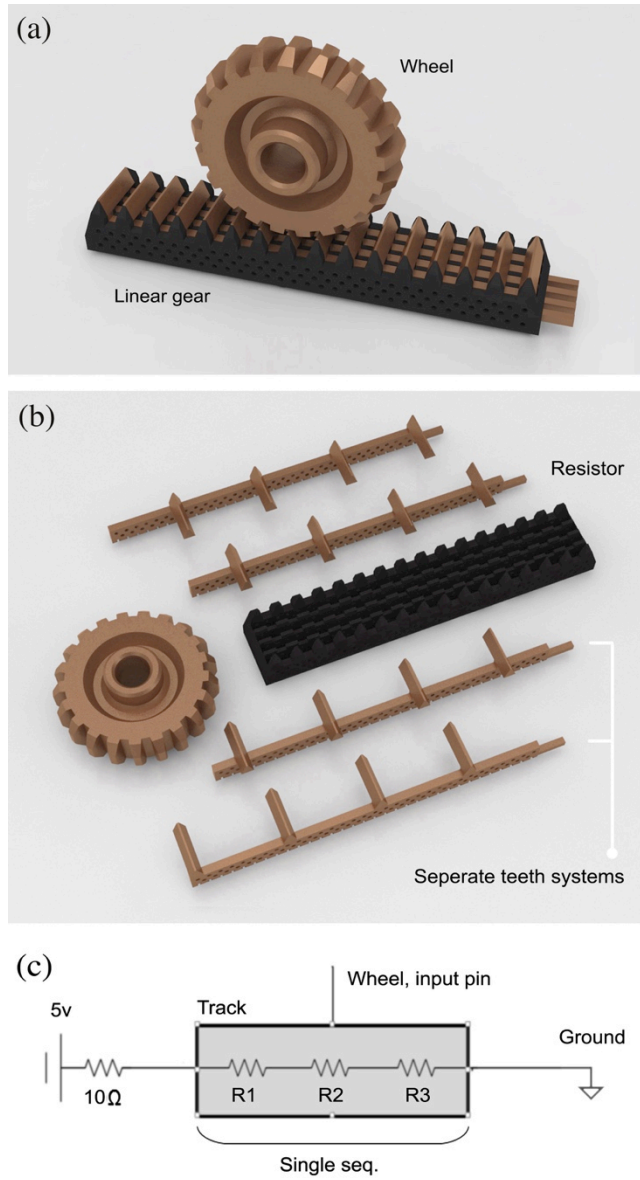

Figure 7. (a-b) The design of the 3D printed voltage divider gear (c), using the conductivity/resistance of the nylon-carbon SLS enclosure. Rendered in VRay.

track, with a different voltage value for every position (see Fig 7). Since the shape of our resistor is complex and the current flows along many paths, it is hard to calculate the resistance numerically. Therefore, the resistance and voltage were determined empirically from measurements. Because the resistance values vary between sequences, the expected voltage levels vary as well. As the variance is bounded by 0.25V, we associate ranges of that size to each position.

The wheel itself is connected to an analog pin on the Arduino board, which reads the outgoing voltage from the circuit. The firmware routinely samples the voltage at the input pin to determine the position of the wheel on the track as it rests between two of the teeth. Since the track provides different resistance values, the level of voltage on the input

pin readings can fall into four different ranges, each corresponding to a position on the track. We assume that the starting position of the wheel is at the first series of resistors. Between every fourth and fifth tooth on the track, the resistance reverts from 5V to 0V, beginning a new sequence. In order to prevent the gear wheel from shorting the 5V pin of the Arduino when moving through this position, a small resistor (10Ohm) buffers between the Arduino's ground pin and its 5V pin.

The firmware samples the voltage on the analog input every 2ms, and provides a reading that averages the values of the previous five samples. The value of the reading is translated to a location (index) on the track by a lookup table, and then output to the serial port. Grasshopper reads this value and converts it to angle and distance in order to rotate and translate the gear model to its corresponding location on the track model.

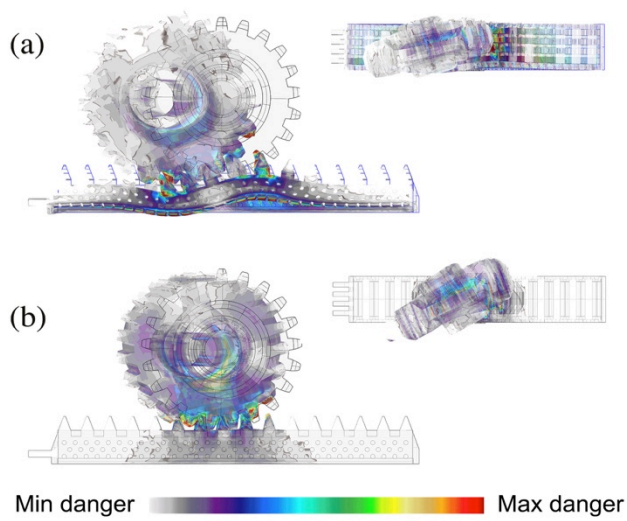

Figure 8. FEM simulation of torque (100KNm) applied to the gear wheel, aligned with the rotation plane, tested on our design (a) and compared to a standard design (b). Colors represent risk (danger) to structural integrity.

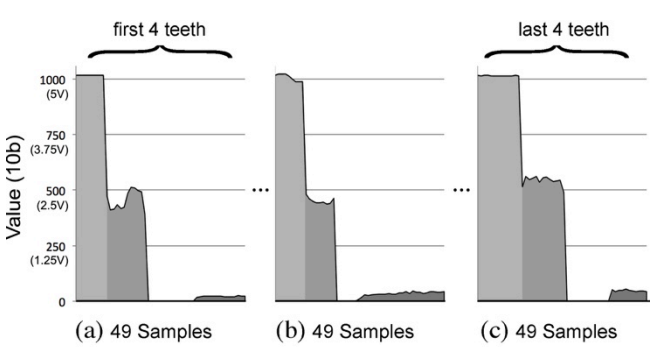

Figure 9. Voltage measurements of the gear wheel transitioning between the teeth on the track, taken from three different sets of teeth.

Gear Performance

As with the ball bearing, an FEM simulation (Fig. 8) supplies initial structural analysis of the gear performance, simulating torque applied to the wheel. Here, the new design fails significantly more often than the traditional design, which has a unified linear gear instead of split teeth. In extreme conditions, the wheel of the traditional design bends a little, while our modified linear gear deforms significantly due to the weak connection of each tooth to its base. This effect can be reduced by using wider teeth that are more strongly connected to their bases and/or by using a side support.

When the wheel is held steady between two teeth on the track, the sampled voltage varies by approximately 0.025V, (at 50HZ). Therefore, a narrow average (only a few samples before and after) is enough for a reliable estimation of the gear's position, unlike the results from the ball bearing. This has a direct effect on the sensors' response time. The smaller the sampling intervals and number of samples for which it averages the values, the more sensitive it is to rapid changes.

As the resistance values are not identical between the resistor sequences, the voltage readings obtained are not identical either. Since the firmware is unaware of the existence of sequences, this necessitates a wider window of accepted values that can be mapped to each position. The size of the windows is different for each position. Fig. 9 shows the voltage values distribution for the different positions.

Machine Element (3): A Variable Capacitor Hinge

A hinge allows an angle of rotation between two elements, and usually consists of a circular bearing mechanism between two joints. It can connect many different elements and come in a wide variety of shapes and sizes. We present a variable capacitor hinge that relies on the device's circular bearing (using 45.6mm from the hinge's total length of 65mm), where one rounded conductive surface (4.2mm radius) moves around a second conductive rounded surface (4.95mm radius). As these surfaces move, their overlapping areas (the capacitor's terminals) change, thus changing the potential capacitance between them (see Fig. 10). By measuring the device's capacitance, we can determine the angle of the hinge.

Capacitance normally depends on the dimensions and design of the device's terminals, the distance between them, and the dielectric constant of an insulator. Like the rest of the printed devices in this paper, we used bronze printing for the conductive parts of the hinge. For the insulator, we chose NyTek™ 1200 GF SLS (nylon 12 and glass). This material has a dielectric constant of 6.3 (where nylon 12 has only around 3 [23]), due to the glass particles. This significantly improved the capacitance of our hinge, and thus its angular resolution.

The capacitance of our hinge ranges from 5pF to 22pF. To get a reliable measurement for these values, we took advantage of the Arduino's inner capacitance. The Arduino's analog pin acts as a second capacitor with a known value. For the Arduino UNO boards we use, this

value is approximately 30pF [20]. Another capacitor is connected in series to the capacitor under test. The inner capacitor may be charged or discharged by changing the output to high or low, respectively. As both capacitors are connected in series, raising the pin to 5V causes current to flow through both. Once the voltage between them settles close to its final value (approximately 30ns), it can be sampled and used to determine the capacitance of the unknown capacitor. In stable state $C_1 = V_{out}C_2/(V_{in}-V_{out})$ where C_2=23pF, V_{in}=5V and C_1 is our unknown capacitor.

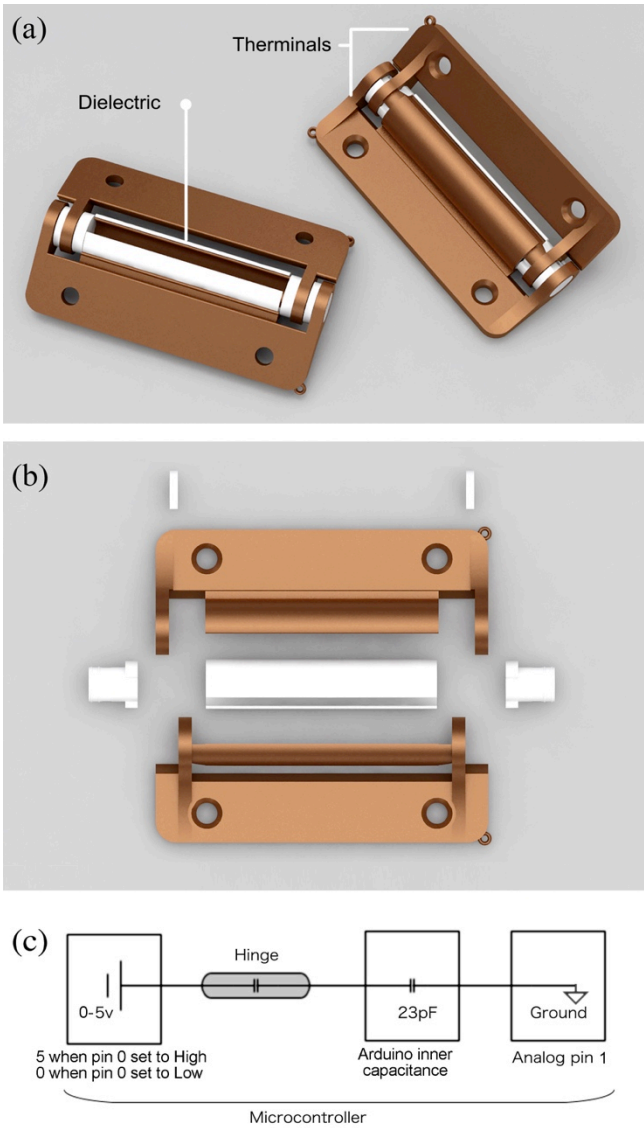

Figure 10. (a-b) The design of the 3D-printed varying capacitance hinge and its analog circuit (c), using the improved dialectic constant of a nylon-glass SLS insulator cylinder. Rendered in VRay.

The firmware charges the capacitors by setting the output pin to high. It sets the input pin to input mode and samples the voltage between the two capacitors. The capacitance is deduced from the sample using the equation described above. The angle of the hinge is then derived from the capacitance with a third-degree polynomial, obtained using Matlab's *polyfit* on 20 capacitance samples from one cycle of opening the hinge from 0 to 180 degrees.

For angle A and capacitance c the relation is given by $A(c) = -0.0189c^3+0.7265c^2-14.5779c+160.3188$. After calculating the angle, the firmware sets the output pin to low, and the input pin to output mode in order to discharge the capacitors before the next measurement cycle, and waits 300ms for the system to stabilize. The wait time, greater than needed to discharge, is a safety measure to avoid starting the cycle with a charged capacitor, which could damage the microcontroller.

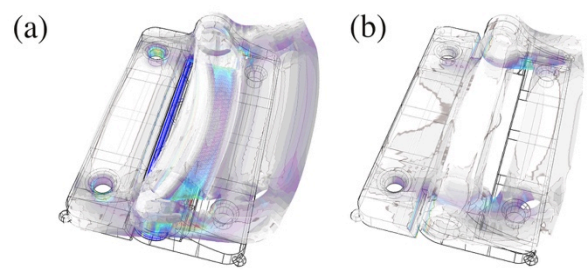

Figure 11. FEM simulation of force applied to the hinge (10KN, pushing apart its two terminals), tested on our design (a) and compared to a standard design (b). Colors represent risk (danger) to structural integrity.

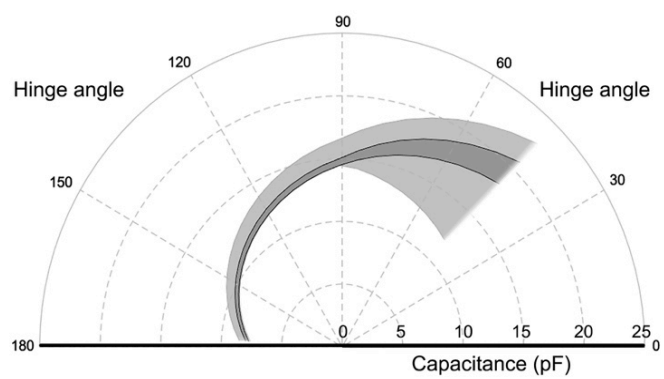

Figure 12. Capacitance values of the hinge measured by the Arduino as a function of the hinge's opening angle. The continuous values were (linearly) interpolated from three data points (45, 90 and 180 degrees). The dark color represents the mean and standard deviation around them, where most of the data found.

Hinge Performance

Because a significant percentage of the hinge's bearing is used for the variable capacitor (instead of operating as a close reinforced rotating axis), it weakens the structural performance of the device, as seen in the FEM simulation (Fig. 11). The tradeoff between the strength and capacitance of the device is obvious. Future development of AM materials with a higher dielectric constant will enable major improvements, allowing a reduction in the terminals' length.

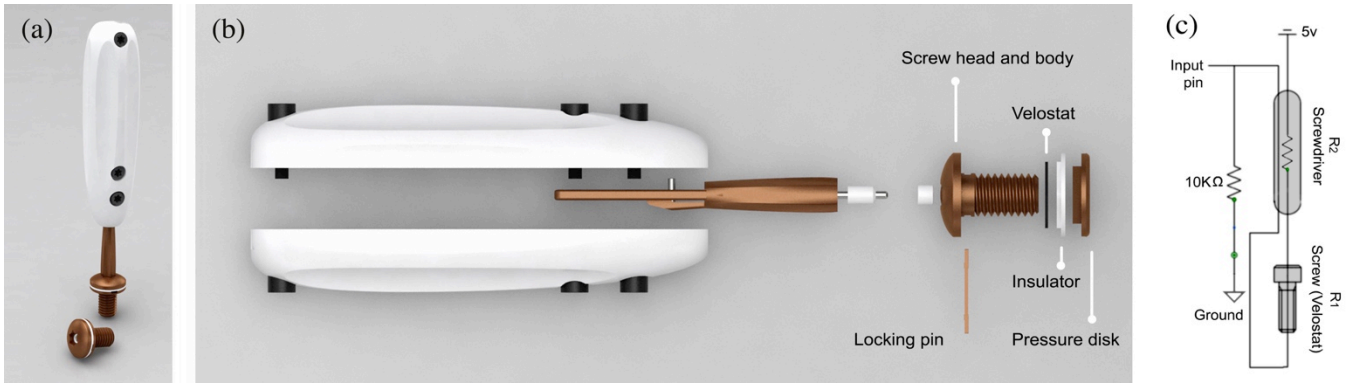

Figure 13. (a-b) The design of the 3D-printed Velostat pressure-sensing screw and its screwdriver and analog circuit (c). Rendered in VRay.

The capacitance measurement obtained from the hinge while it holds at a steady angle fluctuates by approximately 1pF. The relation of capacitance to angle is not linear. Rather, as the angle decreases, the change in capacitance becomes less significant. Fig.12 contains shows the samples taken over 15 seconds at 45, 90, and 180 degrees.

Machine Element (4): A Velostat Screw

Many applications require the stress applied by or on a screw to be precisely tuned. However, the relevant information necessary to make these adjustments is not always available. Unlike our earlier devices, here we chose to rely on an existing sensing material and embed it in our design. Velostat is a thin (0.1mm) pressure-sensitive conductive material: squeezing it will reduce the resistance [25]. We designed a 3D-printed screw (see Fig. 13) with a special disk isolated from the main body of the screw, located between the screwhead and the base surface (the radius of the screwhead being 7.9mm). Three layers of Velostat sheets were placed between this ring and the screwhead. When the screw is driven into a surface, it changes its resistance due to pressure applied to the ring. A special 3D-printed screwdriver can read this pressure while driving the screw (see. Fig 14).

Since the screw changes its resistance as pressure is applied, the best way to deduce its resistance at a given time is by using a simple voltage divider circuit. To measure its value, we connect the screw in series to a 5KOhm resistor (using the special screwdriver) and supply it with an incoming voltage of 5V. For the unknown resistor R_1, a resistor with a known value R_2=5K, input voltage V_{in}=5V, and the sampled voltage V_{out}, we can easily find $R_1 = R_2(V_{in}/V_{out}-1)^{-1}$. In a similar vein with the previous components, the firmware samples the V_{out} every 100ms and averages the result with the adjacent samples, after which it calculates the resistance with the given formula. A simple Grasshopper program displays a visualization of the change in the screw's location, based on the assumption that a rise in pressure indicates change in position.

Screw Performance

Compared to traditional screw design, the additional ring we place underneath the screwhead does not significantly weaken the screw's structure. Only when the screwhead is subjected to an extreme (and unrealistic) pressure can we detect some differences in the FEM simulation between our design and a traditional (unified) one (see Fig. 15). We do not consider this a significant concern.

The resulting sensor is very sensitive. A slight change in pressure on the screw is enough to change its resistance in the realm of KOhms. Therefore, the electrical output must be toned down to achieve a workable data set. Fig. 16 shows the voltage obtained for various levels of pressure on the screw. Any change in voltage represents KOhms of change in resistance. As the evaluation reveals, the screw is highly sensitive to a value range of 125-750g. Further evaluation is recommended for higher values.

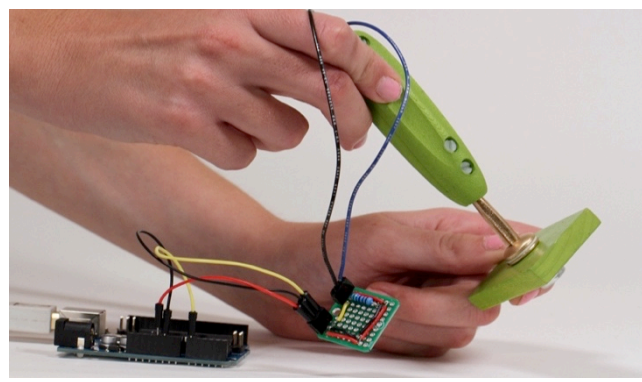

Figure 14. Operation scenario of the Velostat screw and the dedicated screwdriver, which is designed to read the information from the screw while driving it.

Design Process and Constraints

Steel-Sense is a hybrid design paradigm relying on traditional design and fabrication tools. We envision an integration of our technical paradigm within an existing design-flow, rather than suggesting a new process. Thus, the design process, limitations and constraints of Steel-Sense are equal to those of the selected 3D printing technology. The scale and resolution of the hybrid elements are bounded only by the fabrication process. For example, as the resolution of the ball bearing is determined by the number of pins embedded in the outer ring, the designer can decide to add more pins if space allows.

Alternatively, a shorter distance between the hinge terminals can improve its capacitance. However, this distance is a factor of the 3D-printed dielectric, and with current SLS technologies, wall thickness cannot be thinner than 0.8mm.

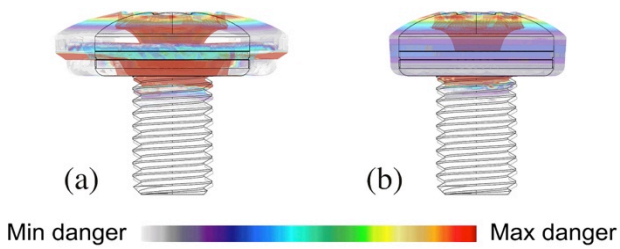

Figure 15. FEM simulation of torque applied to the screw (500KNm), in the direction of the screwing axis, tested on our design (a) and compared to a standard design (b). Colors represent risk (danger) to structural integrity.

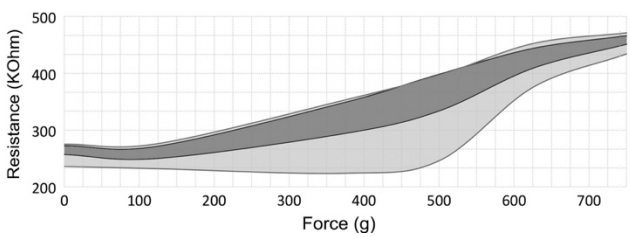

Figure 16. Voltage values of the screw measured by the Arduino as a function of applied force (measured at 0, 125, 375, 500, 625 & 750 g). The plot is a spline interpolation. The dark color represents the mean with the standard deviation around it, where most of the data found.

Generally speaking, the 3D printing process falls short compared to the accuracy of traditional machining, and our AM elements lack the operational smoothness of common machine elements. Until the accuracy of AM improves, this can be solved by post-machining the elements via milling, lathing, drilling, etc., as is already done for high-end DMLS parts. Additionally, while using our bare hands to work with the printed elements, we noted unstable electronic behavior caused by the conductivity of our skin affecting the sensors. For future real-world applications, we recommend that such hybrid elements be insulated.

IMPLICATIONS FOR THE DESIGN OF INPUT DEVICES

Today, digital fabrication technologies contribute to a growing portfolio of new designs, interactions and technical solutions. Many new interactive scenarios require compact sensing solutions to control and improved performance. Additionally, many applications need small mechanical and sensorial solutions to improve their designs and lower their cost while merging the physical with the virtual. Here, we review potential applications for Steel-Sense, considering the different principles we presented and different production costs.

Professional, high-end hybrid solutions Considering the high production costs of DMLS, we believe the main professional application for Steel-Sense is in custom, one-off solutions that require unique designs. As the main applications of DMLS technologies are already in producing unique one-offs for special needs [15], we hope our work will inspire designers and engineers to reconsider the designs of these and other hybrid-printed parts, introducing entirely new possibilities for designing interactive machines.

For example, the ball bearing demonstrates a seamless integration principle: without affecting the mechanical properties of the bearing structure, we augment the element with new sensorial capabilities. Such a design could be ideal for high-end, professional mountain or road bicycles. As these bicycles use expensive fabrication technologies and composite materials to gain improved performance, the high cost of DMLS may not be a significant barrier for this application. A titanium DMLS ball bearing could sense wheel movement very accurately, without the need to attach external sensing devices that can add weight, impact the aerodynamic design of the bicycles, and be easily damaged if not fully enclosed. Moreover, such a ball bearing could be custom designed to fit unique requests, integrating it as part of a wider in-wheel system. By tracking both wheels in this way, riders, coaches, and designers could collect valuable information and analyze it to improve performance.

3D-printed custom mechatronics Steel-Sense contributes a new design principle, showing how standard 3D printing materials can be used to implement capacitors and resistors: a 3D-printed nylon-carbon composite can function as a resistor, and a nylon-glass composite as a dialectic. Together with 3D-printed conductors and insulators, these enable the design of complicated forms and structures that can implement capacitive sensors, voltage dividers, varying resistors and capacitors, and more. While we presented a simple gear-voltage divider that can ease the integration of sensing within space-tight 3D-printed gears, we believe the potential here is much wider. Thus, we will explore it farther in our future work. One example is in developing fully interactive, 3D-printed mechatronics, or 3D-printed custom transmitter-receiver devices. Using one of the less expensive options for 3D printing metals would keep costs low, making these applications relevant to many DIY projects.

The shift from virtual to physical in HCI encouraged researchers to investigate different designs and scenarios for physical interactive prototypes [8], many of them made using AM [19]. Haptic input devices [5] harness physical degrees of freedom for sensing, with a virtual model that reacts to physical action. As these haptic devices contain bearings and hinges, this is a good use case for considering various capacitor solutions. Moreover, while we have presented a varying capacitor hinge, a similar concept can be applied to a telescopic arm, using one of the cheaper metal 3D printing options. Together, they would enable easy DIY design and rapid prototyping of custom haptic

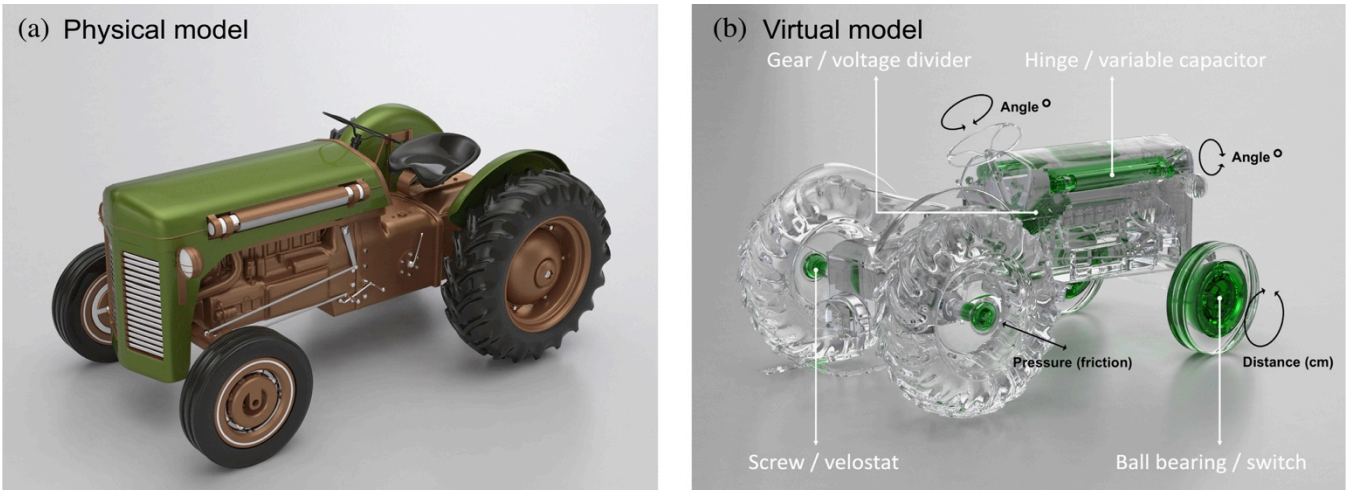

Figure 17. A futuristic concept design for a two-worlds ((a) physical, (b) virtual) model of a 3D-printed tractor toy which has all of our machine element designs embedded as integral parts: ball-bearings in the front wheels to measure distance; a voltage divider gear to detect the angle of the steering wheel; a variable capacitor hinge to report whether the engine doors are open, and by how much; and a screw that can apply pressure to the back wheels (and report on it) to add friction and slow them down. Both figures were rendered in VRay.

scanners, relying on angular and linear degrees of freedom, as an example of 3D printed mechatronics.

Mass-production of machine elements While this paper focuses on the affordances of 3D printing, the implications of Steel-Sense go beyond the AM realm. A direct example relies on our pressure sensor screw. While a screw is a simple element, many people do not use it properly. We envision our 3D-printed design evolving into a mass-produced smart screw product, rather than a solely custom design solution. For example, if a user drives a screw too hard, it may crack wooden surfaces; in a cement plaster wall, over-screwing can destroy the threads of the screw holes. While a simple application inside a smart screwdriver can solve these problems, we believe such a solution may also lead to broader applications. A screw element that can report on its own pressure through a screwdriver agent invites us to conceptualize new opportunities. Just as recent developments in computer graphics seek ways to assist in design, construction and assembly of furniture [2, 16], intelligent construction elements such as screws can virtually mirror the building process and supply real-time instructions and alarms in potentially dangerous situations.

Integrated System As an example of future integrated implications for Steel-Sense, Fig. 17 shows a concept design for a 3D-printed tractor toy that has all of our machine elements designs embedded as integral parts of the tractor. A virtual model mirrors the physical one, relying on the data received from the sensors. As interactive compact physical/virtual toys are already common [24], we believe applications like this one may receive great benefits from the Steel-Sense hybrid design paradigm. Using one of the cheaper metal 3D printed options mentioned earlier, DIY toys can easily be tracked and control virtual scripts, sharing their physical performance and recording it for future use, learning, and interactive scenarios.

CONCLUSIONS

This paper presents Steel-Sense, a new approach to augmenting machine elements with sensing capabilities using AM. While machine elements act in the physical domain, and sensors are used to report on the virtual one, our hybrid elements suggest a new integrated territory. We contribute a hybrid design paradigm, illustrated by 3D-printed metal parts to facilitate both sensors and machine elements in a single component. We present four design primitives, implementing (1) an electronic switch, (2) a voltage divider, (3) a variable capacitor, and (4) an existing sensing material (Velostat) embedded inside 3D-printed machine elements. In addition, we build simple analog/digital systems, mirroring the physical devices and their performance in the virtual (PC) environment. Our evaluations show that while there are a few technical limitations that can be improved, the designs are reliable and stable, and fulfill our initial motivation.

We see the potential of Steel-Sense to contribute wise, compact, customable and interactive mechatronics to HCI. We envision this new family of hybrid elements impacting the traditional design of interactive system, as they offer a new interactive vocabulary. Moreover, Steel-Sense presents a new paradigm of interactive units equipped to *perform* while *measuring*. To articulate the potential of these hybrid units for HCI and design, we hope to farther develop a theoretical framework for this new design space and describe how it interacts with traditional design paradigms.

ACKNOWLEDGMENTS

We deeply appreciate all the friends and colleagues who supported and assisted us in completing this work: N.W. Gong, P. Schmitt, R. Fattal, G. Ron, J. A. Paradiso, M. Feldmeier, M. Mizrahi, S, Olberding and C. L. Evers.

REFERENCES

1. Athreya, S. R., Kalaitzidou, K., Das, S. 2010. Processing and characterization of a carbon black-filled electrically conductive Nylon-12 nanocomposite produced by selective laser sintering. Materials Science and Engineering: A, 527, Issues 10–11, 25 April 2010. doi:10.1016/j.msea.2009.12.028

2. Fu, C.W., Song, P., Yan, X., Yang, L.W., Jayaraman, P.K., and Cohen-Or, D. 2015. Computational interlocking furniture assembly. ACM Trans. Graph. 34, 4, Article 91 (July 2015), 11 pages. DOI=http://dx.doi.org/10.1145/2766892

3. Gershenfeld, N. 2007. Fab: The Coming Revolution on Your Desktop--from Personal Computers to Personal Fabrication. Basic Books (February 6, 2007).

4. Gong, N.-W., Steimle, J., Olberding, S., Hodges, S., Gillian, N., Kawahara, Y., and Paradiso, J. A. 2014. PrintSense: a versatile sensing technique to support multimodal flexible surface interaction. In Proceedings of the SIGCHI Conference on Human Factors in Computing Systems (CHI '14). ACM, New York, NY, USA, 1407-1410. DOI=http://dx.doi.org/10.1145/2556288.2557173

5. Geomagic® Haptic Devices website. 2015. Retrieved at September 25, 2015 from http://www.geomagic.com/en/products-landing-pages/haptic

6. Gong, N.-W., Zoran, A. and Paradiso, J. A. 2013. Inkjet-printed conductive patterns for physical manipulation of audio signals. In Proceedings of the adjunct publication of the 26th annual ACM symposium on User interface software and technology (UIST '13 Adjunct). ACM, New York, NY, USA, 13-14. DOI=http://dx.doi.org/10.1145/2508468.2514932.

7. Innovative Products - SENSOR BEARINGS FOR INDUSTRIAL MACHINERY. NSK Europe website. Retrieved December 26, 2015, from http://www.nskeurope.com/cps/rde/xchg/eu_en/hs.xsl/innovative-sensor-bearings-for-industrial-machinery.html

8. Ishii, H., Leithinger, D., Follmer, S., Zoran, A., Schoessler, P., and Counts, J. 2015. TRANSFORM: Embodiment of "Radical Atoms" at Milano Design Week. In Proceedings of the 33rd Annual ACM Conference Extended Abstracts on Human Factors in Computing Systems (CHI EA '15). ACM, New York, NY, USA, 687-694. DOI=http://dx.doi.org/10.1145/2702613.2702969

9. Kawahara, Y., Hodges, S., Gong, N.-W., Olberding, S. and Steimle, J. 2014. Building Functional Pervasive Computing Prototypes using Conductive Inkjet Printing. In IEEE Pervasive Computing, (Volume:13 , Issue: 3), July-Sept. 2014. DOI=http://doi.ieeecomputersociety.org/10.1109/MPRV.2014.41

10. Schmitt, P. 2011. Original Machines: Developing Tools and Methods for Object-Oriented Mechatronics. PhD dissertation, Massachusetts Institute of Technology. Dept. of Architecture. Program in Media Arts and Sciences.

11. Shapeways website - 3D Printing Service and Marketplace. (n.d.). Retrieved August 23, 2015, from http://www.shapeways.com/materials/wax

12. Shilkrot, R., Maes, P., Paradiso, J. A., and Zoran, A. 2015. Augmented Airbrush for Computer Aided Painting (CAP). ACM Trans. Graph. 34, 2, Article 19 (March 2015). DOI=http://dx.doi.org/10.1145/2699649

13. Stratasys Direct Manufacturing website - 3D PRINTING & MANUFACTURING. (n.d.). Retrieved August 23, 2015, from https://www.stratasysdirect.com/materials/direct-metal-laser-sintering/

14. Steimle, J. 2015. Printed electronics for human-computer interaction. In ACM Interactions 22, 3 (April 2015), 72-75. DOI=http://dx.doi.org/10.1145/2754304

15. Systems and Solutions for Metal Manufacturing. EOS website. Retrieved August 23, 2015, from http://www.eos.info/systems_solutions/metal

16. The World's First 3D Electronics Printer. Voxel8 website. Retrieved August 23, 2015, from http://www.voxel8.co/

17. Li, H., Hu, R., Alhashim, I., and Zhang, H. 2015. Foldabilizing furniture. ACM Trans. Graph. 34, 4, Article 90 (July 2015), 12 pages. DOI=http://dx.doi.org/10.1145/2766912

18. Motor encoder units. SKF website. Retrieved December 26, 2015, from http://www.skf.com/us/products/bearings-units-housings/engineered-products/sensor-bearing-units/motor-encoder-units/index.html?switch=y

19. Nakagaki, K., Inamura, C., Totaro, P., Shihipar, T., Akikyama, C., Shuang, Y., and Ishii. H. 2015. Linked-Stick: Conveying a Physical Experience using a Shape-Shifting Stick. In Proceedings of the 33rd Annual ACM Conference Extended Abstracts on Human Factors in Computing Systems (CHI EA '15). ACM, New York, NY, USA,1609-1614. DOI=http://dx.doi.org/10.1145/2702613.2732712

20. Capacitance measurement with the Arduino Uno. Nethercott website . Retrieved August 24, 2015, from http://wordpress.codewrite.co.uk/pic/2014/01/21/cap-meter-with-arduino-uno/

21. Niiyama, R., Sun, X., Yao, L., Ishii, H., Rus, D., and Kim, S. 2015. Sticky Actuator: Free-Form Planar Actuators for Animated Objects. International Conference on Tangible, Embedded, and Embodied Interaction (TEI'15), ACM, New York, NY, USA, 77-84. DOI=http://dx.doi.org/10.1145/2677199.2680600

22. Norton, R. L. 2010. Machine Design, (4th Edition), Prentice-Hall.

23. Material Properties of SLS Thermoplastics. JR Prototypes website. Retrieved August 23, 2015, from http://www.jrprototypes.com/sls-prototypes/sls-material-properties.htm

24. Patkar, M. (2013, September 10). 8 Cool Smartphone-Controlled Toys You Secretly Desire! Retrieved August 23, 2015, from http://www.makeuseof.com/tag/8-cool-smartphone-controlled-toys-you-secretly-desire

25. PRESSURE-SENSITIVE CONDUCTIVE SHEET (VELOSTAT/LINQSTAT). (n.d.). Retrieved August 23, 2015, from https://www.adafruit.com/products/1361

26. Yao, L., Niiyama, R., Ou, J., Follmer, S., Silva, C. D., and Ishii, .. 2013. PneUI: pneumatically actuated soft composite materials for shape changing interfaces. In Proceedings of the 26th annual ACM symposium on User interface software and technology (UIST '13). ACM, New York, NY, USA, 13-22. DOI=http://dx.doi.org/10.1145/2501988.2502037

27. Willis, K., Brockmeyer, E., Hudson, S. and Poupyrev, I. 2012. Printed optics: 3D printing of embedded optical elements for interactive devices. In Proceedings of the 25th annual ACM symposium on User interface software and technology (UIST '12). ACM, New York, NY, USA, 589-598. DOI=http://dx.doi.org/10.1145/2380116.2380190

28. Zoran, A. 2011. "The 3D Printed Flute: Digital Fabrication and Design of Musical Instruments," Journal of New Music Research (JNMR), volume 40, issue 4, December 2011.

29. Zoran, A, Shilkrot, R, and Paradiso, J.A. 2013. Human-computer interaction for hybrid carving. In Proceedings of the 26th annual ACM symposium on User interface software and technology (UIST '13). ACM, New York, NY, USA, 433-440. DOI=http://dx.doi.org/10.1145/2501988.2502023